Gas Sensors

International Edition: DOI: 10.1002/anie.201709558
German Edition: DOI: 10.1002/ange.201709558

Layer-by-Layer Assembled Conductive Metal–Organic Framework Nanofilms for Room-Temperature Chemiresistive Sensing

*Ming-Shui Yao[+], Xiao-Jing Lv[+], Zhi-Hua Fu, Wen-Hua Li, Wei-Hua Deng, Guo-Dong Wu, and Gang Xu**

Abstract: *The utility of electronically conductive metal–organic frameworks (EC-MOFs) in high-performance devices has been limited to date by a lack of high-quality thin film. The controllable thin-film fabrication of an EC-MOF, $Cu_3(HHTP)_2$, (HHTP = 2,3,6,7,10,11-hexahydroxytriphenylene), by a spray layer-by-layer liquid-phase epitaxial method is reported. The $Cu_3(HHTP)_2$ thin film can not only be precisely prepared with thickness increment of about 2 nm per growing cycle, but also shows a smooth surface, good crystallinity, and high orientation. The chemiresistor gas sensor based on this high-quality thin film is one of the best room-temperature sensors for NH_3 among all reported sensors based on various materials.*

Electronic conductive metal–organic frameworks (EC-MOFs) are a newly emerging type of porous conductive material.[1] Compared with traditional porous conductive materials, such as porous carbons and porous metals, EC-MOFs possess a crystalline state, narrow size distribution and regularly arranged pores, tunable band gap, and a designable charge transport pathway.[2] EC-MOFs have shown great potential applications as field-effect transistors (FETs), supercapacitors, thermoelectric devices, oxygen reduction reaction electrocatalysts (ORRs), and chemiresistor gas sensors.[1b,2a,b,3] Up to now, the major EC-MOFs based devices are fabricated with powders or thick films.[2b,3d,e] Nevertheless, a large grain size and bad grain contact inhibit the fast transport of both electron and mass in above electrical devices. To improve further the performances of these devices, a high-quality EC-MOFs film with controllable thickness on a nanometer (and less than 100 nm) scale is required.[3c,4] Unfortunately, the fabrication of a EC-MOF thin film with good control in nanometer scale over thickness, grain size, roughness, and orientation, as far as we know, has not been achieved yet.

Herein, we report the controllable thin film fabrication of an EC-MOF, $Cu_3(HHTP)_2$, by a spray layer-by-layer (LbL) liquid-phase epitaxial method for the first time. The thin film not only can be precisely prepared with a thickness increment of about 2 nm in each growing cycle, but also shows a smooth surface, good crystallinity, and high orientation. These good qualities of the EC-MOF thin film facilitate its application in high-performance semiconductor devices. As a proof of concept, high-performance chemiresistor gas sensors based on $Cu_3(HHTP)_2$ thin films were fabricated and studied.

The crystal structure of $Cu_3(HHTP)_2$ is shown in Figure 1 a. In the *ab* plane, Cu ions coordinate to HHTP ligands to form a two-dimensional (2D) hexagonal layer. The hexagonal layers pack along the *c*-axis in a slipped-parallel AB stacking model with an interval distance of 3.3 Å, resulting in a honeycomb-like porous structure. The one-dimensional channels have an open-window size of about 1.8 nm and a large amount of polar organic functional groups on the wall. The strong charge delocalization between Cu ions and ligands endows this MOF with good electronic conductivity. To prepare $Cu_3(HHTP)_2$ thin film, the substrates (for example, sapphire, glass, Si/SiO_2, quartz) were firstly treated with Piranha solution to obtain −OH functionalized surface (Supporting Information, Figure S1). After that, the function-

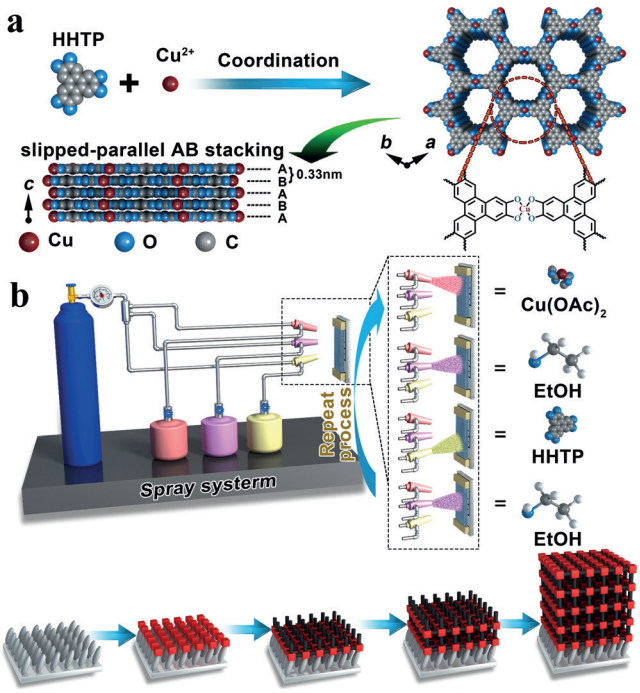

Figure 1. Illustration of a) the crystal structure of $Cu_3(HHTP)_2$ and b) the preparation of $Cu_3(HHTP)_2$ thin-film gas sensors.

[*] Dr. M. S. Yao,[+] X. J. Lv,[+] Dr. Z. H. Fu, W. H. Li, W. H. Deng, Dr. G. D. Wu, Prof. G. Xu
State Key Laboratory of Structural Chemistry, Fujian Institute of Research on the Structure of Matter, Chinese Academy of Sciences (CAS)
155 Yangqiao Road West, Fuzhou, Fujian, 350002 (P. R. China)
E-mail: gxu@fjirsm.ac.cn
[+] These authors contributed equally to this work.

Supporting information and the ORCID identification number(s) for the author(s) of this article can be found under: https://doi.org/10.1002/anie.201709558.

alized substrates were alternatively exposed to the ethanolic solution of copper(II) acetate (0.1 mM) and the HHTP ligands (0.01 mM) to epitaxially grow $Cu_3(HHTP)_2$ thin film in a LbL fashion by a spray method (Figure 1b; for details, see the Supporting Information).[5] In this work, it was found that −OH groups can play the similar role of the organic self-assembly-monolayer to orient the MOF thin film growth. Between each spray steps, the substrate was rinsed with pure ethanol to remove unreacted reactants, which makes the thin film growth controllable in thickness. With various growing cycles, the $Cu_3(HHTP)_2$ thin films with different thickness were obtained, which were denoted as $Cu_3(HHTP)_2$-xC (*x* is the growing cycles).

Figure 2a and b show the scan electron microscope (SEM) and atomic force microscopy (AFM) images of the typical top and cross-sectional view of the $Cu_3(HHTP)_2$-40C thin film. The observed thin film is dense and continuous. Similar results can be found for the thin films with different growing cycles (Supporting Information, Figure S2). Owing to its higher resolution at vertical dimension, AFM was employed to further confirm the thickness of the thin films with growing cycles less than 40 (Supporting Information, Figure S3). Figure 2c shows the linear relationship between the growing cycle and the thickness of the thin film, which reveals the precisely controlled growth of $Cu_3(HHTP)_2$-xC with average 2 nm increment in thickness for each growing cycle. AFM measurements further confirm the smooth and continuous surfaces for all $Cu_3(HHTP)_2$-xC (Figure 2b; Supporting Information, Figure S4). The calculated root mean square (RMS) surface roughness increases depending on the thickness of $Cu_3(HHTP)_2$-xC, but the highest value is less than 5 nm for the thin film with 100 nm thickness (Figure 2d). The smooth growing process can be further confirmed by monitoring $Cu_3(HHTP)_2$-xC on quartz substrate with a UV/Vis spectrum. As shown in Figure 2e, the absorbance of the thin film increases with increasing the growing cycles. The intensity of the maximum absorption peak (366 nm) is linearly proportional to the growing cycles, which is consistent with these observed by SEM and AFM measurements. The powder X-ray diffraction (PXRD) spectrum shows the pattern of the prepared $Cu_3(HHTP)_2$-50C matches well with that simulated from the crystal structure of $Cu_3(HHTP)_2$ (Figure 2f), demonstrating the successful preparation of $Cu_3(HHTP)_2$-xC.

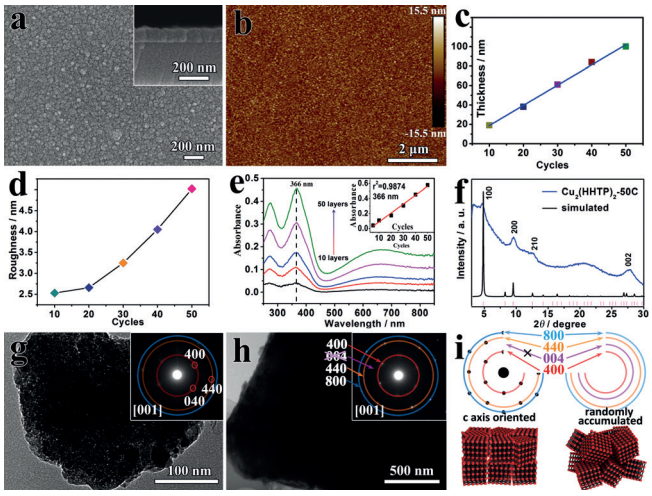

Figure 2. Top views of $Cu_3(HHTP)_2$–40C: a) SEM image (inset: cross-sectional view) and b) AFM image; c)–e) growing-cycle-dependent c) thickness, d) roughness, and e) UV/Vis spectra of $Cu_3(HHTP)_2$-xC (inset: cycle-dependent intensity of absorbance at 366 nm); f) PXRD patterns of as prepared $Cu_3(HHTP)_2$-50C (blue) and simulation (black); g),h) TEM images and corresponding SAED patterns of fragments of g) $Cu_3(HHTP)_2$-10C and h) $Cu_3(HHTP)_2$-50C; i) simulated SAED patterns of *c*-axis oriented and randomly accumulated particles.

The orientation nature of $Cu_3(HHTP)_2$-xC was revealed by using transmission electron microscope (TEM) measurements. Selected area electron diffractions (SAED) of the thin film fragments peeled off from $Cu_3(HHTP)_2$-10C and $Cu_3(HHTP)_2$-50C match the hexagonal crystal structure of $Cu_3(HHTP)_2$ ($a = b = 21.75$ Å, $c = 6.66$ Å),[2a,3b] further confirming the crystalline phase and purity of $Cu_3(HHTP)_2$-xC (Figure 2g and h). Since the thickness of $Cu_3(HHTP)_2$-10C is about 20 nm and that of $Cu_3(HHTP)_2$-50C is about 100 nm, which are much smaller than the observed lateral sizes of the thin film fragments for TEM measurement ($Cu_3(HHTP)_2$-10C > 300 nm, $Cu_3(HHTP)_2$-50C > 5000 nm), the fragments should be peeled off parallel to the substrate. So the orientation of these fragments should be the same as that of $Cu_3(HHTP)_2$-xC. The SAED patterns exhibit oriented-polycrystal-like dots arrays and the diameter of the electron beam used for SAED measurement is around 500 nm, which indicates the single crystal domain size in the thin film is up to hundreds nm. The rings of (*hk*0) can be clearly observed, while the rings of (00l) are missing from the pattern. Similar results could be found on randomly selected other fragments (Supporting Information, Figure S5). These results strongly imply the *c*-axis orientation structure feature of $Cu_3(HHTP)_2$-xC (Figure 2i). Determining the orientation by SAED method has been demonstrated feasible on textured ZnO seeds thin film[6] and layered salts thin film.[7]

Ammonia (NH_3) is a toxic, flammable, and explosive gas but utilized extensively in chemical industries, fertilizer factories, and so on.[8] It is also a typical biomarker for the detection of kidney and liver diseases[9] for breath analysis.[10] At present, realizing high sensitive and selective detection of NH_3 at room temperature (RT) is still a big challenge. In view of its high RT conductivity of 0.02 S cm^{-1} (Supporting Information, Figure S6), $Cu_3(HHTP)_2$-xC were utilized to fabricate chemiresistor sensors for the NH_3 detection of high sensitivity and selectivity. $Cu_3(HHTP)_2$-xC based chemiresistor sensors (Supporting Information, Figure S1a) were tested in a home-made sensing system reported in our previous works (for details, see the Supporting Information).[11] Figure 3a shows the typical response–recovery curve of $Cu_3(HHTP)_2$-10C to NH_3 with different concentrations. Upon exposure to NH_3, the sensor resistance exhibited a pronounced increment, which is the typical behavior of a p-type semiconductor. The current curve presents good response-recovery to a broad range of the NH_3 concentrations (1 to 100 ppm). Good repeatability of response to 100 ppm NH_3 with low coefficient of variation (1.54%) can be observed. The average resistance change of $Cu_3(HHTP)_2$-10C toward 100 ppm NH_3 was estimated to be 129%. It is about 12 times

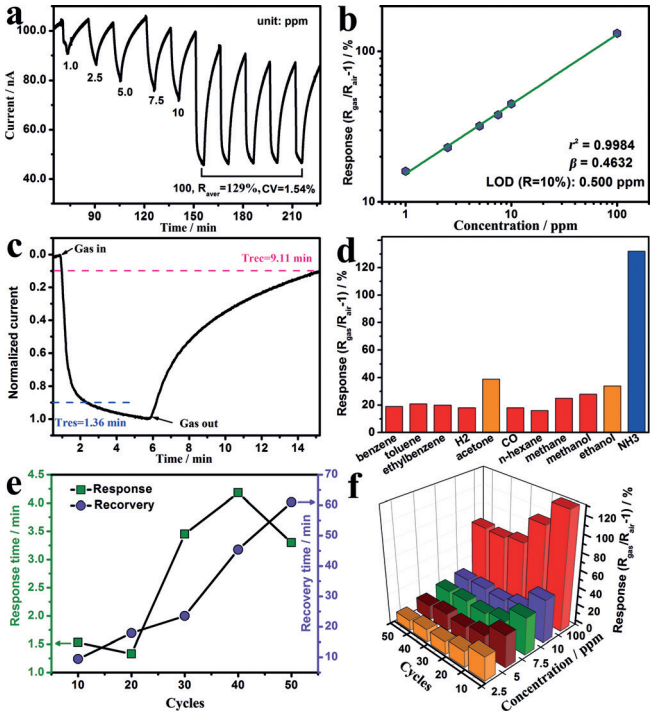

Figure 3. RT gas-sensing performances of $Cu_3(HHTP)_2$-xC: a) the response–recovery curve toward NH_3 with different concentrations, b) response–concentration log–log plots, c) response–recovery time curves to 100 ppm NH_3, and d) column chart of responses toward different reducing gases of $Cu_3(HHTP)_2$-10C, e),f) growing-cycle-dependent e) response–recovery time comparison to 100 ppm NH_3 and f) responses comparison to NH_3 with different concentrations.

higher than that of the reported sensors based on $Cu_3(HHTP)_2$ powders[3e] or nanorods,[3f] and about 5 times higher than the $Cu_3(HHTP)_2$ thick-film gas sensor (Supporting Information, Figures S7, S8). Notably, this response value is among the highest ones of the reported RT sensors (Supporting Information, Table S1).

Figure 3b shows the log–log plots of response ($R_{gas}/R_{air}-1$) vs. concentration of $Cu_3(HHTP)_2$-10C sensor toward NH_3. The good linearity in the range of 1 to 100 ppm is in accordance with typical chemiresistor gas sensor.[11] A β value of 0.472 is close to 0.5, which is generally indicative of a fully regular microstructure of the nanograins ($\beta > 0.5$, disordered microstructure; $\beta < 0.5$, local agglomeration or zones).[12] The theoretical limit of detection (LOD) can be calculated to be about 0.5 ppm from the simulated linear equation by setting the response to be 10%.[13] Figure 3c illustrates the response time (the time required increasing the resistance to 90% of the saturation value) and recovery time (the time required decreasing the saturated resistance to its 10%) of $Cu_3(HHTP)_2$-10C when exposed to 100 ppm NH_3 and dry synthetic air, respectively. Fast response and recovery times with the values of 1.36 and 9.11 min can be estimated, respectively. Compared with a $Cu_3(HHTP)_2$ powder-based sensor, the response and recovery of $Cu_3(HHTP)_2$-10C are speeded up by 54% and 10%, respectively (Supporting Information, Figure S7). Notably, the response speed of $Cu_3(HHTP)_2$-10C is among one of the fastest value for various reported NH_3 RT gas sensors (Supporting Information, Table S1), which might be further improved by introducing proper foreign metal ions or organic ligand that have relatively weaker interactions with NH3 into $Cu_3(HHTP)_2$ and by further improving the quality of the thin film.

The cross-sensitivities of $Cu_3(HHTP)_2$-10C toward 100 ppm of typical reducing gases were shown in Figure 3d. The sensor showed responses lower than 20% toward most of these gases. Even for RT highly active gas molecules, such as acetone and ethanol, they can only induce responses between 30% and 40%. The value of selectivity (S = Response (NH_3)/Response (gas)) of NH_3 toward different reducing gas varied from 4.55 to 8.25, which is good enough for precise detection of NH_3 among these interfering gases.

The effect of the thickness to the sensor performances was systemically evaluated via conducting growing cycle-dependent gas-sensing measurements. As shown in Figure 3e and the Supporting Information, Figure S9, faster response and recovery of thinner film can be clearly observed due to the easier contact of guest molecules with the active sites with minimal diffusion barriers in these films. For sensors with growing cycles of 30 or higher, their response–recovery speed were even lower than these of powder based sensor (Supporting Information, Figure S7), because the powder one possesses a significant amount of macro/meso-pores owing to loose accumulation of crystallites for relatively better gas diffusion. It is also observed that the thinner films have the higher responses to NH_3.

$Cu_3(HHTP)_2$-xC sensors have excellent long-term stability and reproducibility. After 3 months, $Cu_3(HHTP)_2$-10C remains 88.4% of its original response towards NH_3 (Supporting Information, Figure S10). The log–log plots of response vs. concentration collected from four sensors for each thickness (10, 30 and 50 growing cycles; Supporting Information, Figure S11) have good linearity and narrow error bars during the sensing measurements of NH_3 with different concentrations (Figure 3f).

Although the exact mechanism for the sensing performances of $Cu_3(HHTP)_2$-xC is still under revealing, we found that 1) the crystal structure of $Cu_3(HHTP)_2$ remains unchanged before and after exposed to saturated NH_3 gas, as observed from PXRD spectra (Supporting Information, Figure S7b); and 2) FTIR spectra (Figure 4a) show typical peaks for NH_3-Cu at 3170, 877, and 856 cm^{-1} as well as a red-shift of ν(C=O) and ν(C–O).[14] These results suggest strong interactions between NH_3 and the framework of $Cu_3(HHTP)_2$, which might be the origin for the high selectivity of $Cu_3(HHTP)_2$ to NH_3. Similar results has also been reported by Dincă[3e] and Mirică's groups.[3f] Ultraviolet photoelectron spectroscopy (UPS) measurements show the Fermi level of $Cu_3(HHTP)_2$-10C increased by 1.13 eV after adsorption of NH_3 (Figure 4b). This is a typical phenomenon when a n-type doping happen to a p-type semiconductor.[15] $Cu_3(HHTP)_2$ is a p-type sensor material and holes dominate its charge transport. The recombination between the hole in $Cu_3(HHTP)_2$ and the doped electron from analytes decreases carrier concentration and increases the resistance of the sensor.[3e,15,16] $Cu_3(HHTP)_2$-xC is very thin (< 100 nm), which provides short gas diffusion length and high ratio of accessible

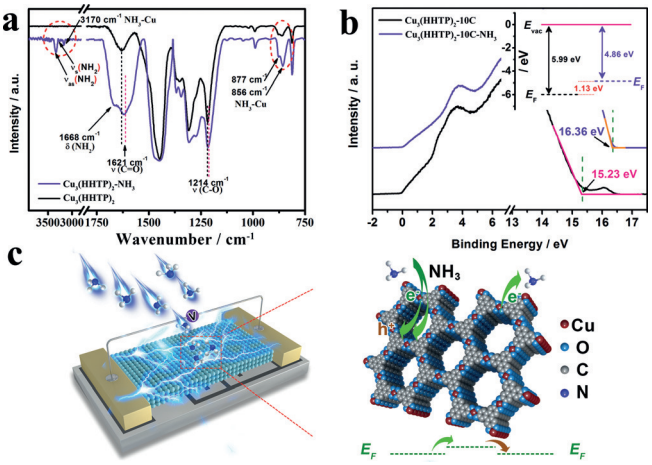

Figure 4. $Cu_3(HHTP)_2$-xC gas sensing mechanism: a) FTIR spectra; b) UPS results (the inset is the calculated band alignment); c) the gas sensor and possible gas-sensing mechanism.

surface area. Moreover, $Cu_3(HHTP)_2$-xC has a high crystallinity and a large single-crystal domain size, which can facilitate effective charge transport. All of these contribute to the high performances of our sensors.

In summary, the controlled preparation of the high-quality thin film based on an electronically conductive MOF, $Cu_3(HHTP)_2$, was reported for the first time. With a spray LbL assembly method, the thin films prepared not only possess good crystallinity and high orientation, but also large crystal domain size, dense packing, smooth surface, and well-controlled thickness. The $Cu_3(HHTP)_2$ thin film with a thickness of 20 nm has excellent room-temperature sensing performances: selective detection of NH_3 toward 10 typical interference gases; highest response with the average resistance change toward 100 ppm NH_3 as high as 129%; very short response time with the value of 1.36 min; and an excellent long-term stability and reproducibility with 88.4% response retention after 3 months. These results indicate the potential application of a RT MOF sensor for real-time monitoring and a timely alarm of toxic, explosive, and flammable NH_3. Since MOF materials can be flexibly designed to obtain high affinity and unique selectivity to target gas, MOF based chemiresistor sensors offer a high possibility to detect a single gas at RT, providing an exciting and powerful platform for the development of new electrical devices.

Acknowledgements

This work was supported by the National Natural Science Foundation of China (21773245, 21401193), the Strategic Priority Research Program of CAS (XDB20000000), Key Research Program of Frontier Science, CAS (QYZDB-SSW-SLH023), Scientific Research and Equipment Development Project, CAS (YZ201609), and the Natural Science Foundation of Fujian Province (2016J06006, 2015J01230, 2016J05053, 2017J05034).

Conflict of interest

The authors declare no conflict of interest.

Keywords: electronic conductivity · gas sensors · metal–organic frameworks · porous structures · thin films

How to cite: *Angew. Chem. Int. Ed.* **2017**, *56*, 16510–16514
Angew. Chem. **2017**, *129*, 16737–16741

[1] a) L. Sun, M. G. Campbell, M. Dincă, *Angew. Chem. Int. Ed.* **2016**, *55*, 3566–3579; *Angew. Chem.* **2016**, *128*, 3628–3642; b) M. Hmadeh, Z. Lu, Z. Liu, F. Gándara, H. Furukawa, S. Wan, V. Augustyn, R. Chang, L. Liao, F. Zhou, E. Perre, V. Ozolins, K. Suenaga, X. Duan, B. Dunn, Y. Yamamto, O. Terasaki, O. M. Yaghi, *Chem. Mater.* **2012**, *24*, 3511–3513; c) A. A. Talin, A. Centrone, A. C. Ford, M. E. Foster, V. Stavila, P. Haney, R. A. Kinney, V. Szalai, F. El Gabaly, H. P. Yoon, L. François, M. D. Allendorf, *Science* **2014**, *343*, 66–69; d) X. Huang, P. Sheng, Z. Y. Tu, F. J. Zhang, J. H. Wang, H. Geng, Y. Zou, C. A. Di, Y. P. Yi, Y. M. Sun, W. Xu, D. B. Zhu, *Nat. Commun.* **2015**, *6*, 7408; e) L. E. Darago, M. L. Aubrey, C. J. Yu, M. I. Gonzalez, J. R. Long, *J. Am. Chem. Soc.* **2015**, *137*, 15703–15711; f) G. K. H. Shimizu, J. M. Taylor, S. Kim, *Science* **2013**, *341*, 354–355.

[2] a) M. G. Campbell, D. Sheberla, S. F. Liu, T. M. Swager, M. Dincă, *Angew. Chem. Int. Ed.* **2015**, *54*, 4349–4352; *Angew. Chem.* **2015**, *127*, 4423–4426; b) D. Sheberla, J. C. Bachman, J. S. Elias, C. J. Sun, Y. Shao-Horn, M. Dincă, *Nat. Mater.* **2017**, *16*, 220–224; c) T. Kambe, R. Sakamoto, K. Hoshiko, K. Takada, M. Miyachi, J.-H. Ryu, S. Sasaki, J. Kim, K. Nakazato, M. Takata, H. Nishihara, *J. Am. Chem. Soc.* **2013**, *135*, 2462–2465; d) S. Takaishi, M. Hosoda, T. Kajiwara, H. Miyasaka, M. Yamashita, Y. Nakanishi, Y. Kitagawa, K. Yamaguchi, A. Kobayashi, H. Kitagawa, *Inorg. Chem.* **2009**, *48*, 9048–9050; e) J. Cui, Z. Xu, *Chem. Commun.* **2014**, *50*, 3986–3988; f) D. Chen, H. Xing, Z. Su, C. Wang, *Chem. Commun.* **2016**, *52*, 2019–2022.

[3] a) G. Wu, J. Huang, Y. Zang, J. He, G. Xu, *J. Am. Chem. Soc.* **2017**, *139*, 1360–1363; b) W. Li, K. Ding, H. Tian, M. Yao, B. Nath, W. Deng, Y. Wang, G. Xu, *Adv. Funct. Mater.* **2017**, *27*, 1702067; c) K. J. Erickson, F. Leonard, V. Stavila, M. E. Foster, C. D. Spataru, R. E. Jones, B. M. Foley, P. E. Hopkins, M. D. Allendorf, A. A. Talin, *Adv. Mater.* **2015**, *27*, 3453–3459; d) E. M. Miner, T. Fukushima, D. Sheberla, L. Sun, Y. Surendranath, M. Dincă, *Nat. Commun.* **2016**, *7*, 10942; e) M. G. Campbell, S. F. Liu, T. M. Swager, M. Dincă, *J. Am. Chem. Soc.* **2015**, *137*, 13780–13783; f) M. K. Smith, K. E. Jensen, P. A. Pivak, K. A. Mirică, *Chem. Mater.* **2016**, *28*, 5264–5268; g) R. Huang, Y. Wei, X. Dong, X. Wu, C. Du, S. Zang, T. C. W. Mak, *Nat. Chem.* **2017**, *9*, 689–697; h) Q. Yang, Q. Xu, H. Jiang, *Chem. Soc. Rev.* **2017**, *46*, 4774–4808; i) K. Choi, H. Jeong, J. Park, Y. Zhang, J. Kang, O. M. Yaghi, *ACS Nano* **2014**, *8*, 7451–7457.

[4] a) S. Wang, Q. Wang, X. Feng, B. Wang, L. Yang, *Adv. Mater.* **2017**, DOI: https://doi.org/10.1002/adma.201701898; b) V. Stavila, C. Schneider, C. Mowry, T. R. Zeitler, J. A. Greathouse, A. L. Robinson, J. M. Denning, J. Volponi, K. Leong, W. Quan, M. Tu, R. A. Fischer, M. D. Allendorf, *Adv. Funct. Mater.* **2016**, *26*, 1699–1707; c) J. J. Richardson, M. Björnmalm, F. Caruso, *Science* **2015**, *348*, aaa2491; d) R. Salunkhe, Y. V. Kaneti, J. Kim, J. Kim, Y. Yamauchi, *Acc. Chem. Res.* **2016**, *49*, 2796–2806.

[5] a) O. Shekhah, H. Wang, M. Paradinas, C. Ocal, B. Schuepbach, A. Terfort, D. Zacher, R. A. Fischer, C. Woell, *Nat. Mater.* **2009**, *8*, 481–484; b) Z. G. Gu, H. Fu, T. Neumann, Z. X. Xu, W. Q. Fu, W. Wenzel, L. Zhang, J. Zhang, C. Wöll, *ACS Nano* **2016**, *10*, 977–983.

[6] L. E. Greene, M. Law, D. H. Tan, M. Montano, J. Goldberger, G. Somorjai, P. Yang, *Nano Lett.* **2005**, *5*, 1231 – 1236.
[7] M. Yao, P. Hu, Y. Cao, W. Xiang, X. Zhang, F. Yuan, Y. Chen, *Sens. Actuators B* **2013**, *177*, 562 – 569.
[8] a) N. A. Travlou, K. Singh, E. Rodríguez-Castellón, T. J. Bandosz, *J. Mater. Chem. A* **2015**, *3*, 11417 – 11429; b) X. Liu, T. Ma, N. Pinna, J. Zhang, *Adv. Funct. Mater.* **2017**, DOI: https://doi.org/10.1002/adfm.201702168; c) H. J. Lin, J. P. Baltrus, H. Gao, Y. Ding, C. Y. Nam, P. Ohodnicki, P. X. Gao, *ACS Appl. Mater. Interfaces* **2016**, *8*, 8880 – 8887.
[9] a) S. Davies, P. Spanel, D. Smith, *Kidney Int.* **1997**, *52*, 223 – 228; b) M. Z. Dai, Y. L. Lin, H. C. Lin, H. W. Zan, K. T. Chang, H. F. Meng, J. W. Liao, M. J. Tsai, H. Cheng, A. Chem, *Anal. Chem.* **2013**, *85*, 3110 – 3117.
[10] S. Kim, S. Choi, J. Jang, H. Cho, I. Kim, *Acc. Chem. Res.* **2017**, *50*, 1587 – 1596.
[11] M. Yao, W. Tang, G. Wang, B. Nath, G. Xu, *Adv. Mater.* **2016**, *28*, 5229 – 5234.
[12] a) N. Hongsith, E. Wongrat, T. Kerdcharoen, S. Choopun, *Sens. Actuators B* **2010**, *144*, 67 – 72; b) H.-J. Kim, J.-H. Lee, *Sens. Actuators B* **2014**, *192*, 607 – 627.
[13] R. W. J. Scott, S. M. Yang, N. Coombs, G. A. Ozin, D. E. Williams, *Adv. Funct. Mater.* **2003**, *13*, 225 – 231.
[14] a) T. Yu, T. Hao, D. Fan, J. Wang, M. Shen, W. Li, *J. Phys. Chem. C* **2014**, *118*, 6565 – 6575; b) L. Ma, Y. Cheng, G. Cavataio, R. W. McCabe, L. Fu, J. Li, *Appl. Catal. B* **2014**, *156*, 428 – 437.
[15] a) K. Y. Ko, J. G. Song, Y. Kim, T. Choi, S. Shin, W. L. Chang, K. Lee, J. Koo, H. Lee, J. Kim, *ACS Nano* **2016**, *10*, 9287 – 9296; b) A. Tarasov, S. Zhang, M. Y. Tsai, P. M. Campbell, S. Graham, S. Barlow, S. R. Marder, E. M. Vogel, *Adv. Mater.* **2015**, *27*, 1175 – 1181.
[16] H. Liu, X. Li, L. Chen, X. Wang, H. Pan, X. Zhang, M. Zhao, *J. Phys. Chem. C* **2016**, *120*, 3846 – 3852.

Manuscript received: September 15, 2017
Accepted manuscript online: October 26, 2017
Version of record online: November 15, 2017

